Available online at www.sciencedirect.com
ScienceDirect
Journal of the European Ceramic Society 27 (2007) 3171–3176
www.elsevier.com/locate/jeurceramsoc

Crystallization kinetics and magnetic properties of iron oxide contained $25Li_2O–8MnO_2–20CaO–2P_2O_5–45SiO_2$ glasses

Chi-Shiung Hsi [a], Huy-Zu Cheng [b,*], Hui-Ju Hsu [b], Yung-Sheng Chen [b], Moo-Chin Wang [c]

[a] *Department of Materials Science and Engineering, National United University, Miao-Li 36003, Taiwan*
[b] *Department of Materials Science and Engineering, I-Shou University, Kaohsiung 803, Taiwan*
[c] *Department of Fragrance and Cosmetics, Kaohsiung Medical University, 100 Shi-Chuan 1st Road, Kaohsiung 807, Taiwan*

Received 19 July 2006; received in revised form 17 November 2006; accepted 25 November 2006
Available online 9 February 2007

Abstract

With crystallization at 850 °C for 4 h, $LiMn_2O_4$, β-wollastonite (β-$CaSiO_3$), lithium silicate (Li_2SiO_3), Ca(Ca, Mn)Si_2O_6 and $Li_2Ca_4Si_4O_{13}$ phases were found in $25Li_2O–8MnO_2–20CaO–2P_2O_5–45SiO_2$ (LMCPS) glass ceramics. The (Li, Mn)ferrite phase was obtained in the iron oxide contained LMFCPS glass ceramic and $Li_2FeMn_3O_8$ phase was found in that containing 8 at.% Fe_2O_3. TEM investigations showed that (Li, Mn)ferrite particles dispersed in the β-wollastonite matrix (Li, Mn)ferrite particles, with an average size of 40 nm, were found in the glass ceramics containing 4 at.% Fe_2O_3. The (Li, Mn)ferrite particle sizes in the glass ceramics containing 8 at.% Fe_2O_3 varied from a few μm to 5 nm. The SQUID result showed that only the glass ceramic containing 4 at.% Fe_2O_3 exhibited super-paramagnetic behavior at temperature 300 K and ferromagnetic behavior at 4 K. The LMCPS glass ceramic containing 8 at.% Fe_2O_3 exhibited ferromagnetic behavior at both temperatures.

Keywords: Crystallization; Glass ceramics; Magnetic properties; Super-paramagnetism

1. Introduction

Glass-ceramics has been developed for use in biological implants. These materials require strict composition and morphology control and the interpenetration mode of the various crystalline and glass phases involved. Since Hench et al.[1] first discovered Bioglass® in 1970', various glasses and glass ceramics have been well established including apatite glass ceramics (Ceravital®)[2] and $Na_2O–CaO–SiO_2–P_2O_3$ bioglasses.[3] Kokubo et al.[4] prepared an apatite–wollastonite (A–W) glass ceramic comparable to natural bone. This glass ceramic exhibits better mechanical properties than other bioceramics[4,5] and is able to form strong bonds with bone.[4] Currently, ferromagnetic phase content bioceramics have been widely used as bone fillers and introduced for hyperthermia treatment.[5–7] Iron oxide nanoparticles have been applied in biomedical applications.[8,9]

A $MgO–CaO–Al_2O_3–SiO_2–P_2O_5$ glass-ceramic with high mechanical strength has been reported by Wu and Hon.[10] Small apatite particles precipitate and anorthite crystals form on the surface of P_2O_5 rich glassceramics.[11] Luderer et al.[12] used lithium ferrite and hematite-containing $Al_2O_3–SiO_2–P_2O_5$ glass ceramics to control tumor growth. A hysteretic heating from the implanted ferromagnetic glass ceramic raised the temperature sufficiently to cause significant tumor growth delay in their investigation. Although the precipitation of magnetic particles from glasses has also been studied by several investigators,[13–15] the devitrification behavior and magnetic properties of LMFCPS glasses have not been elaborated in detail.

The devitrification behavior and magnetic properties of LMFCPS glasses are discussed in this paper. This research studied the phase transformation of LMFCPS glass after crystallization and investigated the magnetic properties of this glass-ceramic system.

2. Experimental procedure

Reagent grade powders of Li_2CO_3, MnO_2, Fe_2O_3, $CaCO_3$, $Ca_3(PO_4)_2$ and SiO_2 were used for preparing the LMFCPS glasses. The glass consisting of 25 at.% Li_2O, 8 at.% MnO_2, 20 at.% CaO, $2P_2O_5$ and 45 at.% SiO_2 were doped with differ-

* Corresponding author.
E-mail address: huyzu@isu.edu.tw (H.-Z. Cheng).

0955-2219/$ – see front matter © 2006 Elsevier Ltd. All rights reserved.
doi:10.1016/j.jeurceramsoc.2006.11.081

ent amounts of Fe_2O_3. They were labeled as F1, F2 and F3 for 0, 4, and 8 at.% Fe_2O_3 addition, respectively. A 100 g raw powder batch of the specified composition was weighed and mixed. These mixed raw materials were melted in a platinum crucible at 1450 °C for 2 h and quenched in water to form amorphous glasses that were subsequently dried and crushed into powder. To obtain a homogeneous glass, the crushed powder was then re-melted at 1450 °C for another 2 h. After the second melting process, the glass was cast onto a 400 °C stainless steel plate and annealed at this temperature for 2–4 h.

Differential thermal analysis (DTA) was conducted in the 25–1000 °C temperature range using a Perkin-Elmer 7 series thermal analyzer with Al_2O_3 powder as the reference material. The crystalline phases formed in the LMFCPS glass ceramics were analyzed using an X-ray diffractometer (XRD, Scintag, XGEN-4000, USA) with Cu Kα radiation and a Ni filter at a scanning rate (2θ) of 2°/min. A scanning electron microscope (SEM, Hitachi S-2700, Tokyo, Japan) was used to observe the microstructure of the glasses and heat-treated samples. The samples were polished, etched with diluted acid solution (5 parts HF, 2 parts HCl and 93 parts distilled water) and coated with a thin conductive film. Thin foils for a scanning transmission electron microscope (STEM, Hitachi HF-2000, Tokyo, Japan) were prepared via the conventional technique: the sample was sliced to a thickness of ~200 μm using a diamond-embedded saw, and then lapped to a thickness of ~30 μm mechanically and ion-beam thinned to electron transparency. Chemical microanalysis was conducted using an energy-dispersive X-ray spectrometer (EDS) (Noran, 432C, USA) attached with STEM. The STEM accelerating voltage was 200 kV. Magnetic measurements were carried out using a superconducting quantum interference device (SQUID) magnetometer with the applied field up to 6 T.

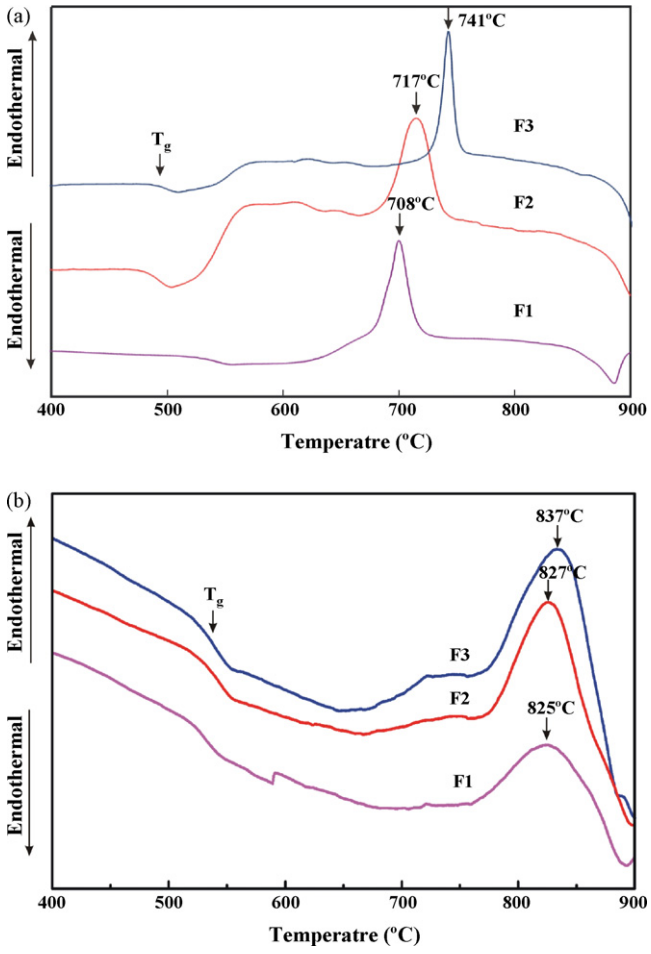

Fig. 1. DTA curves of the LMFCPS glasses heated at a rate of 10 °C/min: (a) powders and (b) bulk.

3. Results and discussion

3.1. Thermal behavior of the LMFCPS glasses

The DTA curves obtained from the LMFCPS glass powders at a heating rate of 10 °C/min are shown in Fig. 1(a). The glass transition temperatures (T_g) were around 480 °C. The T_g refers to the onset of glass transition[16] and corresponds to the temperature at which the network acquires mobility and changes from a rigid into a plastic structure.[17] Moreover, Fig. 1(a) also shows the single glass transition temperature, meaning the existence of a compositionally homogeneous glass state. The exothermic peaks (T_c) were obtained at 708, 717, and 741 °C for F1, F2, and F3 glasses, respectively. High Fe_2O_3 content in the LMFCPS glass, results in high T_c. Fig. 1(b) also shows the DTA result from the LMFCPS glass bulk at a heating rate of 10 °C/min. It indicates that the bulk LMFCPS glasses had exothermic peaks at 825, 827, and 837 °C for F1, F2, and F3 samples, respectively. The exothermic temperatures of the bulk LMFCPS glasses also slightly increased with increasing Fe_2O_3 contents. This result may be caused by the viscosity increase of the LMFCPS with increasing Fe_2O_3 content.

3.2. Crystallization behavior of the LMFCPS glasses

The difference of the exothermic temperature, ΔT_c, between the bulk and powders of the LMFCPS glasses was due to the surface nucleation of the samples since the Fe_2O_3 particle in the glass acts as a nucleation agent accordingly decreases the activation energy. After the F3 glass was crystallized at 600 °C for 4 h and its surface lapped away by 0.1 mm, the XRD pattern showed an amorphous state, as indicated by pattern (a) in Fig. 2. Crystallization at 600 °C for 4 h, $LiMn_2O_4$ was the main phase of F3 bulk sample as illustrated by pattern (b) in Fig. 2. When the surface of the F3 LMFCPS glass was crystallized at 850 °C for 4 h, the $Li_2FeMn_3O_8$ phase was obtained, as shown by pattern (d) in Fig. 2 and disappeared after lapping by 0.1 mm, pattern (c). These results indicated the surface nucleation of the LMFCPS glasses.

According to the XRD result, Table 1 lists the phases formed on the surfaces of the different LMFCPS glasses crystallized at various temperatures. After crystallization at 600 °C for 4 h, $LiMn_2O_4$ was the major phase and β-wollastonite ($CaSiO_3$) was the minor phase in the LMFCPS glass ceramic. The β-wollastonite phase becomes dement when the LMFCPS glasses are crystallized at 640 °C for 4 h, both $LiMn_2O_4$ and

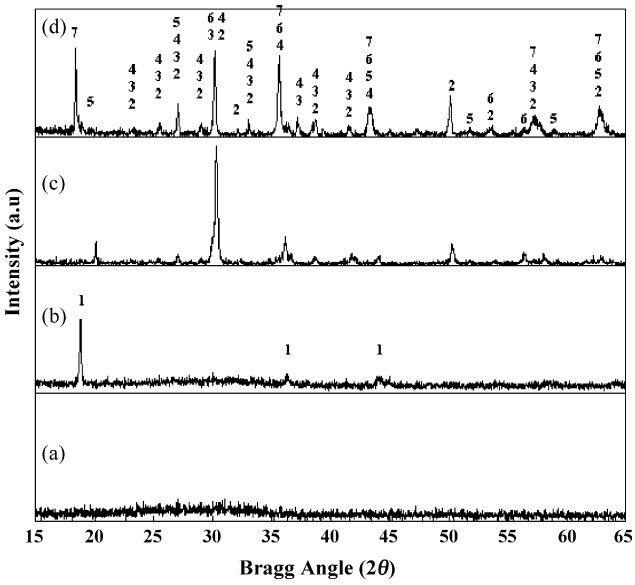

Fig. 2. XRD patterns of the F3 LMFCPS glass crystallized at 600 and 800 °C for 4 h, respectively: (a) 1 μm below the surface of F3 crystallized at 600 °C, (b) the surface of the sample crystallized at 600 °C, (c) 1 μm below the surface of the sample crystallized at 850 °C, and (d) surface of the sample crystallized at 850 °C. (1) $LiMn_2O_4$: JCPDS 35-782; (2) $CuSiO_3$: JCPDS 42-547; (3) $Li_2Ca_4Si_4O_{13}$: JCPDS 37-714; (4) $Ca(Ca, Mn)Si_2O_6$: JCPDS 44-1455; (5) Li_2SiO_3: JCPDS 29-829; (6) (Li, Mn)ferrite; (7) $Li_2FeMn_3O_8$: JCPDS 40-944. *The Joint Committee for Powder Diffraction Studies (JCPDS), founded in 1941 and changed name to International Centre for Diffraction Data (ICDD) in 1978, maintains a database of diffraction patterns. This database designed for use with a diffractometer is often used to identify substances based on X-ray diffraction data.

β-wollastonite were the major phases in the heat-treated sample. When the LMFCPS glasses were crystallized at 660 °C for 4 h, $LiMn_2O_4$, $CaSiO_3$, $Li_2Ca_4Si_4O_{13}$ and $Ca(Ca, Mn)Si_2O_6$ appeared in the glass ceramics. (Li, Mn)ferrite was the minor phase for the F2 and F3 LMFCPS glasses crystallized at 720 °C for 4 h. When the F1 glass was crystallized at 720 °C for 4 h, it showed the same phases as the sample crystallized at 660 °C for 4 h. (Li, Mn)ferrite became evident in the crystallized F2 and F3 LMFCPS glass ceramics, and $Li_2FeMn_3O_8$ formed in the F3 sample when crystallized at 850 °C for 4 h. The crystallized phases in the LMFCPS glass ceramics did not change with dwelling time. When the LMFCPS glasses were crystallized at 720 and 850 °C for 4 h, respectively, Li_2SiO_3 phase presented in all LMFCPS glass ceramic samples and $LiMn_2O_4$ became minor phase in the crystallized F1 and F2 samples. $Li_2FeMn_3O_8$ appeared in the F3 LMFCPS glass ceramic.

According to the EDS analysis the particles in the LMFCPS glass ceramic consist of Fe, Mn, and O. When the F2 and F3 LMFCPS glass crystallized at 850 °C for 4 h, the XRD diffraction angles (2θ) located at 30.26°, 35.68°, 53.66°, 57.24°, 62.76° correspond to iron contended phase, such as $LiFe_5O_8$, $MnFe_2O_4$, and $FeFe_2O_4$, etc. The crystallized F3 sample's diffraction angles were higher than that for $MnFe_2O_4$ and $FeFe_2O_3$, but lower than that for $LiFe_5O_8$. The lattice constant (a) of the iron contended phase could be calculated using the Nelson–Riley equation[18]:

$$a = a_0 - a_0 K \left(\frac{\cos^2\theta}{\sin\theta} + \frac{\cos^2\theta}{\theta} \right) \quad (1)$$

where K is an experimental constant and the second term is the displacement error during the X-ray diffraction measurement.

Table 1
Phases formed on the surface of different LMFCPS glasses crystallized at various temperatures for 4 h

Crystallization temperature (°C)	F1 (0Fe_2O_3 added)	F2 (4Fe_2O_3 added)	F3 (8Fe_2O_3 added)
600	$LiMn_2O_4$	$LiMn_2O_4$	$LiMn_2O_4$
620	$LiMn_2O_4$ $CaSiO_3$(−)	$LiMn_2O_4$ $CaSiO_3$(−)	$LiMn_2O_4$ $CaSiO_3$(−)
640	$LiMn_2O_4$ $CaSiO_3$	$LiMn_2O_4$ $CaSiO_3$	$LiMn_2O_4$ $CaSiO_3$
660	$LiMn_2O_4$ $CaSiO_3$ $Li_2Ca_4Si_4O_{13}$ $Ca(Ca, Mn)Si_2O_6$	$LiMn_2O_4$ $CaSiO_3$ $Li_2Ca_4Si_4O_{13}$ $Ca(Ca, Mn)Si_2O_6$	$LiMn_2O_4$ $CaSiO_3$ $Li_2Ca_4Si_4O_{13}$ $Ca(Ca, Mn)Si_2O_6$
720	$LiMn_2O_4$ $CaSiO_3$ $Li_2Ca_4Si_4O_{13}$ $Ca(Ca, Mn)Si_2O_6$	$LiMn_2O_4$ $CaSiO_3$ $Li_2Ca_4Si_4O_{13}$ $Ca(Ca, Mn)Si_2O_6$ (Li,Mn)Ferrite (-)	$LiMn_2O_4$ $CaSiO_3$ $Li_2Ca_4Si_4O_{13}$ $Ca(Ca, Mn)Si_2O_6$ (Li,Mn)Ferrite (-)
850	$LiMn_2O_4$(−) $CaSiO_3$ $Li_2Ca_4Si_4O_{13}$ $Ca(Ca, Mn)Si_2O_6$ Li_2SiO_3	$LiMn_2O_4$(−) $CaSiO_3$ $Li_2Ca_4Si_4O_{13}$ $Ca(Ca, Mn)Si_2O_6$ Li_2SiO_3 (Li, Mn)ferrite	$Li_2FeMn_3O_8$ $CaSiO_3$ $Li_2Ca_4Si_4O_{13}$ $Ca(Ca, Mn)Si_2O_6$ Li_2SiO_3 (Li, Mn)ferrite

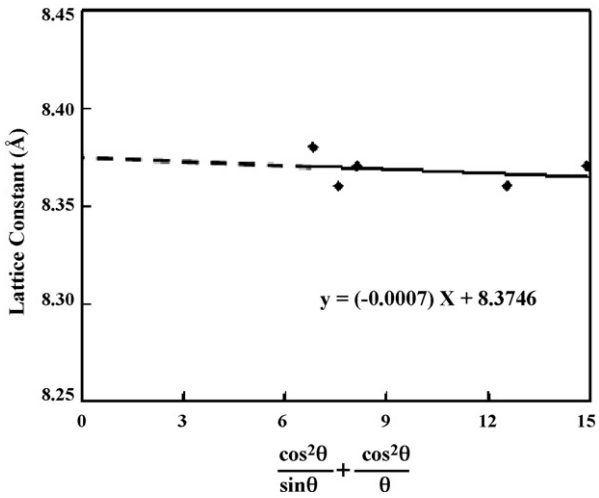

Fig. 3. Nelson–Riley plot of the (Li, Mn)ferrite formed in the LMFCPS glass ceramics.

The lattice constant error (a) is nearly zero when θ approaches 90°.

Using a proper extrapolation function, the lattice constant of the iron-bearing phase in the crystallized LMFCPS glass ceramic had a value of about 8.38 Å as illustrated in Fig. 3. This value was smaller than those for $FeFe_2O_4$ (8.396 Å) and $MnMn_2O4$ (8.499 Å) and was higher than that for $LiFe_5O_8$ (8.337 Å). Therefore, the iron-bearing phase in the crystallized LMFCPS glass ceramic was a solid solution labeled as (Li, Mn)ferrite.

3.3. Microstructure of the LMFPCS glass ceramics

Fig. 4(a) is the SEM micrograph of the F1 LMFCPS glass crystallized at 850 °C for 4 h, indicating that the grey Ca-rich phase and dark Si-rich phase were obtained by phase separation. The Si-rich phase was compatible with the Li_2SiO_3 phase in the F1 glass ceramic. According to the XRD heat-treated sample results listed on Table 1, the Ca-rich phases in the dark area are $CaSiO_3$, $Li_2Ca_4Si_4O_{13}$ and $Ca(Ca, Mn)Si_2O_6$. The Ca-rich phase became columnar and well crystallized with the Fe_2O_3 addition to the LMFCPS glass. The white particles dispersed around the boundaries of the Ca-rich phases in the F2 and F3 crystallized at 850 °C shown in Fig. 4(b) and (c). The white particles had high iron (Fe) content, they determined as (Li, Mn)ferrites and $Li_2FeMn_3O_8$. The higher the iron oxide content in the glass, the more (Li, Mn)ferrites and $Li_2FeMn_3O_8$ it presented. The microstructure of the LMFCPS glass ceramics indicated that its Si-rich phase area decreased with increasing iron oxide content because of the formation of (Li, Mn)ferrites and $Li_2FeMn_3O_8$. The morphology of the crystalline phases in the samples with different LMFCPS glasses crystallized at 850 °C for various holding times was similar.

Fig. 5 shows a STEM micrograph of the F2 LMFCPS glass crystallized at 850 °C for 4 h, it demonstrates that the magnetite particles, columnar β-wollastonite and Si-rich matrix present in this sample. Fig. 6 illustrates the bright field (BF) micrograph and selected area electron diffraction (SAED) patterns of the F2 LMFCPS glass crystallized at 850 °C for 4 h. According to the SAED results, the dark particles and matrix in Fig. 6(a) are identified as (Li, Mn)ferrite (Fig. 6(b)) and $CaSiO_3$ (Fig. 6(c)), respectively. The ferrite particles containing Mn and Fe were also characterized using EDS. Although Li was not found in LMFCPS glass ceramics using EDS, the XRD indicates that the

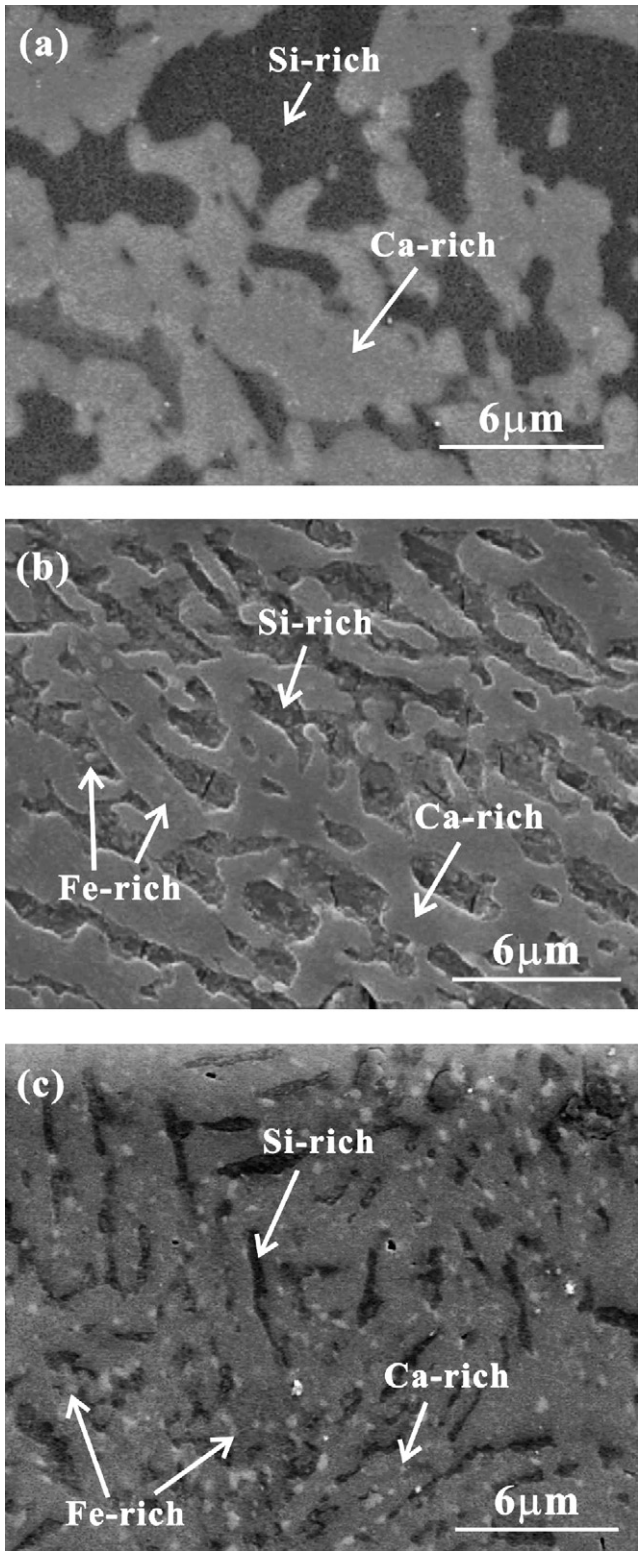

Fig. 4. SEM micrographs of (a) F1, (b) F2 and (c) F3 LMFCPS glasses crystallized at 850 °C for 4 h.

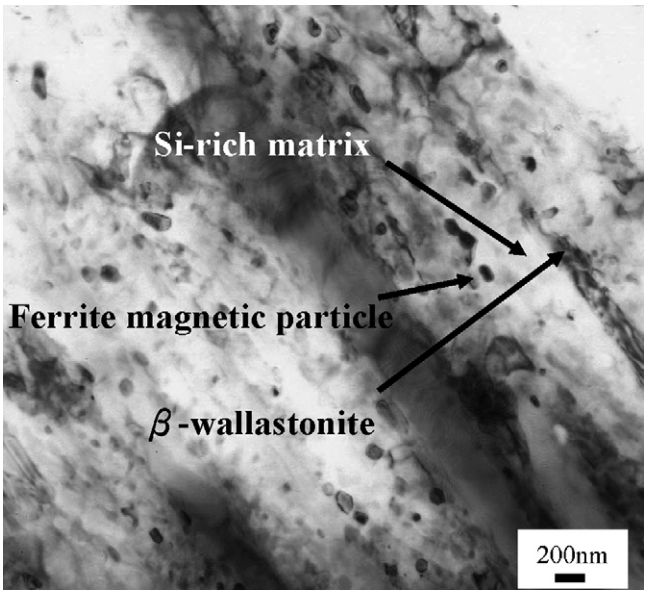

Fig. 5. STEM micrograph of the F2 LMFCPS glasses crystallized at 850 °C for 4 h.

ferrite is considered to be (Li, Mn)ferrite. The ferrite particle size in the crystallized F2 LMFCPS glass ceramic ranges a few nm to 100 nm. Moreover, when the F3 LMFCPS glass crystallized at 850 °C for 4 h, the particle size of the (Li, Mn)ferrite distributed from a few μm to nm.

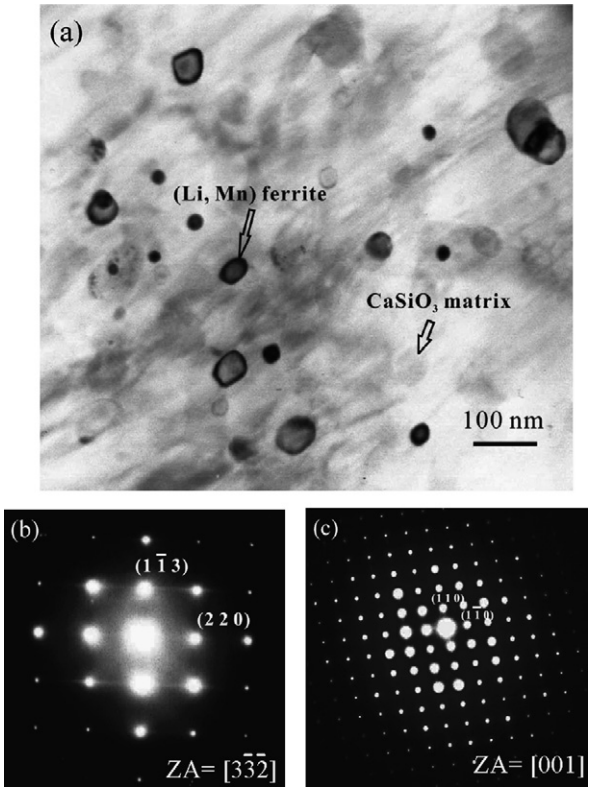

Fig. 6. STEM micrograph of: (a) bright field image, (b) SAED pattern of the (Li, Mn)ferrite with the [3 3̄ 2̄] zone axis (JCPDS 10-319) and (c) β-wollastonite with [0 0 1] zone axis (JCPDS 42-547).

According to the SEM and TEM examinations, the Si-rich phase and β-wollastonite formed in the LMFCPS glass ceramic matrix and the spherical ferrite particles were well dispersed in it. These phases are the three major crystallites in the sample as shown in Fig. 4(b) and (c). In the XRD patterns of the crystallized F2 LMFCPS glasses, (Li, Mn)ferrite, β-wollastonite, and Li_2SiO_3 are obtained. Both the Fe^{2+} and Fe^{3+} are able to enter the wollastonite lattice,[15] with the β-wollastonite matrix composition essentially $CaO{\cdot}SiO_2$. The composition of the glassy phase of the glass ceramic matrix varies with crystallization temperature.

3.4. Magnetic properties of the LMFCPS glass ceramics

Fig. 7 shows the magnetization behavior of the F2 and F3 LMCFPS glasses crystallized at 850 °C for 4 h and measured at temperature of 4 and 300 K. The remanent induction of these samples is less than 0.5 emu/g, which is much smaller than that bulk magnetite (≅92 emu/g).[19] Very small saturation magnetization is obtained due to the modest content of the magnetic phase in the F2 and F3 LMFCPS glass ceramics.[15] The coercive

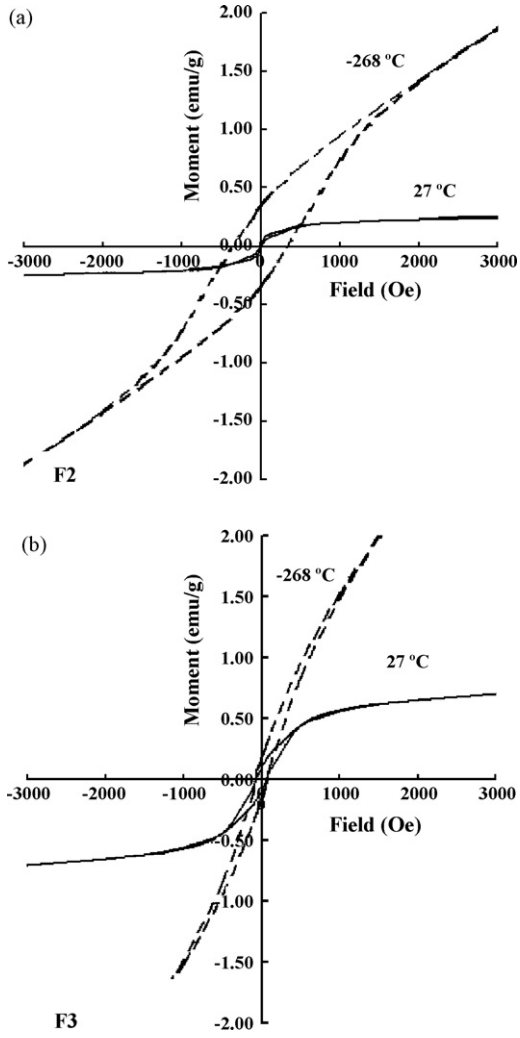

Fig. 7. Magnetization curves of (a) F2 and (b) F3 LMFCPS glasses crystallized at 850 °C for 4 h.

forces of the F2 and F3 LMFCPS glass ceramics measured at 4 K were 338 and 70 Oe, respectively. The iron-containing glass ceramics reveal the ferromagnetic behavior at 4 K. Increasing the measuring temperature to 300 K, the coercive force of the F2 LMFCPS glass ceramic decreases to a value smaller than 5 Oe. The coercive force difference in the F2 LMFCPS glass ceramics measured at 4 and 300 K was larger than 330 Oe, due to the super-paramagnetic effect of this sample.[20] The coercive force of the F3 glass ceramic is 63 Oe at 27 °C, it maintained the ferromagnetic characteristic.

Taketomi and Chikazumi[21] pointed out that the crystallite size determines the coercive force of the glass–ceramics, a single domain structure is formed when the ferrite particle size is of the order of 10–50 nm for moderate crystal anisotropy. Both super-paramagnetic and ferromagnetic characteristics coexisted when the sample contained both large and small particles.[22] The average ferrite particle size in the 850 °C, 4h heat-treated F2 sample was about 40 nm. The coercive force of the sample was only 5 Oe at 300 K, consistent with that by Kuźmiński et al.[22] Therefore, both super-paramagnetic and ferromagnetic behaviors co-existed in the F2 LMFCPS glass ceramics at 300 K. The super-paramagnetic behavior was attributed to those (Li, Mn)ferrites with particle size smaller than 40 nm and the ferromagnetic behavior to those with larger particle size. The particle size of the ferrite in the F3 LMFCPS glass ceramic was in the μm range and thus exhibited ferromagnetic behavior at both temperatures.

4. Conclusions

We have demonstrated a simple technique for preparing (Li, Mn)ferrite nano-particles using the LMFCPS glass ceramic system. The LMFCPS glass ceramics showed surface nucleation behaviors during various heat-treatment processes. The precipitated β-$CaSiO_3$ and Li_2SiO_3 formed with a columnar morphology and the nano-sized (Li, Mn)ferrite particles dispersed in the gray β-$CaSiO_3$ matrix. By varying the weight percentage of Fe_2O_3 in the glass-ceramic we were able to control the (Li, Mn)ferrite grain size. As the (Li, Mn)ferrite grain size in the matrix glass became smaller than 40 nm, the magnetic behavior showed mixed super-paramagnetism and ferro-magnetism in a rather complex way. However, as the grain size grew larger the magnetic behavior changed to ferro-magnetism. The magnetic properties were consistent with the particle size and structure. Magnetic anisotropy constants calculated from our experimental data agree well with the expected values for small particles.

Acknowledgement

The authors would like to thank Dr. S.H. Chien of Academia Sinica and Prof. M.P. Hung of National Cheng Kung University for their discussions with us and Ms. Liang-Chu Wang of National Sun Yat-San University for assistance in TEM. Research support from the National Science Counsel under contract number NSC-92-2216-E-214-008 is sincerely acknowledged.

References

1. Hench, L. L., Splinter, R. J., Allen, W. C. and Greenlee, T. K., Mechanisms of interfacial bonding between ceramics and bone. *Biomed. Mater. Res. Symp.*, 1972, **2**, 117–141.
2. Bromer, H., Deutscher, K., Blencke, B., Pfeil, E. and Strung, V., Properties of the bioactive implant material Ceravital. *Sci. Ceram.*, 1977, **9**, 219–225.
3. Wilson, J., Composites as biomaterials. In *Glass-Current Issues*, ed. A. F. Wright and J. Dupuy. Martinus Nijhof Publishers, Dordyecht, 1985, pp. 662–669.
4. Kokubo, T., Shigematsu, M., Nagashima, Y., Tashiro, M., Nakamura, T., Yamamuro, T. *et al.*, Apatite- and wollastonite-containing glass–ceramics for prosthetic application. *Bull. Inst. Chem. Res. Kyoto Univ.*, 1982, **60**, 260–268.
5. Leventouri, Th., Kis, A. C., Thompson, J. R. and Anderson, I. M., Structure, microstructure, and magnetism in ferromagnetic bioceramics. *Biomaterials*, 2005, **26**, 4924–4931.
6. Arcos, D., del Real, R. P. and Vallet-Regi, M., Biphasic materials for bone grafting and hyperthermia treatment of cancer. *J. Bio-Med. Mater. Res.*, 2003, **65A**, 71–78.
7. Ohura, K., Ikenaga, M., Nakamura, T., Yamamuro, T., Ebisawa, Y., Kokubo, T. *et al.*, A heat-generating bioactive glass–ceramic for hyperthermia. *J. Appl. Biomater.*, 1991, **2**, 153–159.
8. Kim, D. K., Zhang, Y., Voit, W., Rao, K. V., Kehr, J., Bjelke, B. *et al.*, Super-paramagnetic iron oxide nanoparticles for nio-medical applications. *Scripta Mater.*, 2001, **44**, 1713–1717.
9. Lian, G., Lewelling, K., Johnson, M., Dormer, K., Gibson, D. and Seeney, C., Fe_3O_4 magnetite nanoparticles coated by silica for biomedical applications. *Microsc. Microanal.*, 2004, **10**, 536–537.
10. Wu, S. C. and Hon, M. H., Effects of Al/P composition ratio on the crystallization of MgO–CaO–Al_2O_3–SiO_2–P_2O_5 bioglass–ceramic system. *J. Ceram. Soc. Jpn.*, 1993, **101**, 626–629.
11. Wu, S. C., Wang, C. L. and Hon, M. H., Effects of Ca/P ratio on the crystallization of MgO–CaO–Al_2O_3–SiO_2–P_2O_5 glass ceramics. *J. Ceram. Soc. Jpn.*, 1995, **103**, 99–103.
12. Luderer, A. A., Borrelli, N. F., Panzarino, J. N., Mansfitld, G. R., Hess, M., Brown, J. R. *et al.*, Glass–ceramic-mediated, magnetic-field-induced localized hyperthermia: response of a murine mammary carcinoma. *Radiat. Res.*, 1983, **94**, 190–198.
13. O'Horo, M. and Steinitz, R., Characterization of devitrification of an iron-containing glass by electrical and magnetic properties. *Mater. Res. Bull.*, 1968, **3**, 117–126.
14. Komatsu, T. and Soga, N., ESR and Mössbauer studies of the precipitation process of various ferrites from silicate glasses. *J. Mater. Sci.*, 1984, **19**, 2353–2360.
15. Ebisawa, Y., Sugimoto, Y., Hayashi, T., Kokubo, T., Ohura, K. and Yamamuro, T., Crystallisation of (FeO, Fe_2O_3)–CaO–SiO_2 glasses and magnetic properties of their crystallized products. *J. Ceram. Soc. Jpn.*, 1991, **99**, 7–13.
16. Yannacopoulos, S. and Kasap, S. O., Glass transformation phenomena in bulk and film amorphous selenium via DSC heating and cooling scans. *J. Mater. Res.*, 1990, **5**, 789–794.
17. Ray, N. H., Transformation temperature of inorganic oxide glasses. Proceedings of the Ninth International Congress on Glass. *Sci. Technol. Commun.*, 1971, **1**, 633–653.
18. Cullity, B. D. and Stock, S. R., *Elements of X-Ray Diffraction* (*3rd ed.*). Prentice Hall, New Jersey, 2001, p. 367.
19. Smit, J., Wijn, H. P. J. and Ferrites, Philips Technical Library. *Einhoven*, 1959, p.157.
20. Berkowitz, A. E. and Schuele, W. J., Magnetic Properties of Some Ferrite Micro-powders. *J. Appl. Phys.*, 1959, **30**, 134–135.
21. Chikazumi, S., Taketomi, S., Ukita, M., Mizukami, M., Miyajima, H., Setogawa, M. and Kurihara, M., Physics of magnetic fluids. *J. Magnetism Magn. Mater.*, 1987, **65**, 245–251.
22. Kuźmiński, M., Ślawska-Waniewska, A. and Lachowicz, H. K., The influence of superparamagnetic particle size distribution and ferromagnetic phase on GMR in melt spun Cu–Co granular alloys. *IEEE Trans. Magn.*, 1999, **35**, 2853–2855.